Green Chemistry

PAPER

View Article Online
View Journal | View Issue

Cite this: *Green Chem.*, 2017, **19**, 3370

Producing wood-based nanomaterials by rapid fractionation of wood at 80 °C using a recyclable acid hydrotrope†

Huiyang Bian,[a,b] Liheng Chen,*[b,c] R. Gleisner,[b] Hongqi Dai[a] and J. Y. Zhu *[b]

Here we report the unparalleled performance of a novel acid hydrotrope, *p*-toluenesulfonic acid (*p*-TsOH), for the rapid and nearly-complete dissolution of wood lignin below the boiling temperature of water. Up to 85% of birch wood lignin can be solubilized at 80 °C for 20 min. Similar degrees of delignification can only be achieved at 150 °C or higher for over 10 hours using known hydrotropes such as aromatic salts, or for 2 hours using alkaline wood pulping. We fractionated mechanically produced birch wood fibers into a carbohydrate-rich water insoluble solid (WIS) fraction and a spent acid liquor containing mainly dissolved lignin. Dialysis of the fractionated WIS resulted in a small amount of lignin-containing crystalline cellulose nanofibrils (LCCNFs) and a majority of the partially hydrolyzed lignocellulosic solid residue (LCSR) that was subsequently fibrillated into dispersible uniform lignocellulosic nanofibrils (LCNFs). The dissolved lignin can be easily separated through precipitation as dispersible lignin nanoparticles (LNPs) by simply diluting the spent acid liquor to below the minimal hydrotrope concentration (MHC) of *p*-TsOH of approximately 10%. The physical and chemical properties of the LCNF and LNP can be tailored by adjusting the *p*-TsOH fractionation severity as well as the intensity of mechanical fibrillation. The lowest severity experiment, in which approximately 62% birch wood lignin was dissolved, resulted in a thicker (51 nm average height) and more hydrophobic LCNF (water contact angle of 82°) as well as LNP with a larger molecular weight of approximately 7200. The low solubility of *p*-TsOH at ambient temperature can facilitate efficient recovery using commercially proven crystallization technology simply by cooling the re-concentrated spent acid liquor after lignin precipitation. This study presented a promising and green pathway in achieving low-cost and sustainable production of wood based nanomaterials such as LCNF and LNP for developing a biobased economy.

Received 3rd March 2017,
Accepted 6th June 2017

DOI: 10.1039/c7gc00669a

rsc.li/greenchem

Introduction

Lignocellulose based nanomaterials, such as cellulose nanocrystals (CNC), nanofibrils (CNF), and lignin nanoparticles (LNP), are renewable and biodegradable. They are attractive for sustainable economic development. Recent research demonstrated that lignocellulosic nanomaterials (LCNM) have great potential for a variety of applications, such as nanocomposites to replace plastics,[1–4] energy systems,[5] electronics,[6–8] photonics,[9,10] and biomedical systems.[11] However, LCNM are tightly embedded in the cell wall of lignocelluloses and difficult to efficiently fractionate. Developing economical and sustainable fractionation technologies for LCNM production is the key to reap the full benefits of lignocelluloses for an environmentally sustainable future.

Existing technologies for producing CNC and CNF need to use market wood pulps with costs of approximately $1000 per tonne, which substantially increases the product cost and negatively affects commercial utilization. CNC is commonly produced from commercial bleached pulp fibers using concentrated sulfuric acid hydrolysis[12] with low yields of approximately 50%.[13] Although the issue of low yield was addressed recently,[14,15] economic recovery of sulfuric acid and disposal of sulfate remain as challenges. Using concentrated dicarboxylic acid hydrolysis[16–19] to produce CNC addressed many problems associated with using mineral acids such as acid recovery and low CNC thermal stability. The process, however, also needs to use expensive market pulp fibers as feedstock.

[a]*Jiangsu Co-Innovation Center of Efficient Processing and Utilization of Forest Resources, Nanjing Forestry University, Nanjing 210037, China*
[b]*Forest Products Laboratory, U.S. Forest Service, U.S. Department of Agriculture, Madison, WI 53726, USA. E-mail: jzhu@fs.fed.us; Tel: +1-(608) 231-9520*
[c]*Key Laboratory of Biomaterials of Guangdong Higher Education Institutes, Department of Biomedical Engineering, Jinan University, Guangzhou 510632, China. E-mail: lihengchen@jnu.edu.cn*

†Electronic supplementary information (ESI) available. See DOI: 10.1039/c7gc00669a

CNF is commonly produced also from market pulp fibers by mechanical fibrillation, with or without[20–22] chemical[23–25] or enzymatic[26,27] pretreatments. Due to the cost of market pulp, the high energy input for mechanical fibrillation without chemical treatments, the high cost for recovery of chemicals, and the environmental issues associated with certain chemicals, CNF production is also expensive. Currently, small quantities of CNC and CNF were sold from $550 (not for profit, produced by the USDA Forest Products Laboratory) to $1400 kg^{-1} (by commercial vendors for profit) and $110 (pure mechanical processing) to $3300 kg^{-1} (TEMPO oxidation treatment, produced by the USDA Forest Products Laboratory), respectively.

Reported studies on LNP production all used solvents such as ethylene glycol,[28] acetone,[29] tetrahydrofuran (THF),[30] or *N*,*N*-dimethylformamide (DMF),[31,32] to solubilize commercial technical lignin, followed by acidic precipitation,[28,29] hexane precipitation,[31] dialysis,[30] or atomization and drying.[32] While commercial technical lignin is inexpensive and available in large quantities, the use of organic solvents is an environmental concern and increases the LNP cost for solvent recovery, which in turn impedes commercial applications.

Here we report the discovery of the hydrotropic property of *p*-toluenesulfonic acid (*p*-TsOH) for fractionating wood to achieve low cost, sustainable, and integrated production of LCNM along with LNP. *p*-TsOH can solubilize approximately 85% of birch wood lignin at 80 °C for only 20 min, resulting in a cellulose-rich water insoluble solid (WIS) fraction and a spent acid liquor stream containing mainly dissolved lignin. Equivalent delignification using known hydrotropes such as aromatic salts and alkaline wood pulping can only be achieved at 150 °C for over 10 h[33] (or 2 h with catalyst[34]) and 150 °C or higher for 2 h, respectively. As schematically shown in Fig. 1, a small amount of lignocellulosic fibrils can be separated from the WIS through dialysis prior to mechanical fibrillation. The WIS, with or without dialysis, can be used to produce lignin containing CNF (LCNF) by mechanical fibrillation using a low energy input due to the substantial dissolutions of lignin and hemicelluloses and the depolymerization of cellulose. The dissolved lignin can be easily precipitated out in the form of LNP by diluting the spent acid liquor to below the minimal hydrotrope concentration (MHC). Because *p*-TsOH only acts as a catalyst and has a low water solubility at ambient temperature (Fig. S1†), efficient recovery can be accomplished using commercially proven crystallization technology by cooling re-concentrated spent acid solution to achieve environmental sustainability. Previously, we applied *p*-TsOH to hydrolyze hemicelluloses and some disordered cellulose of bleached eucalyptus pulp fibers (near zero lignin content) for the integrated production of CNC with CNF.[16] The hydrotropic property of *p*-TsOH for efficient delignification was not discovered.

The significance of the present study lies in the fact that low cost raw lignocelluloses can be directly used for producing LCNM anticipated to meet the commercial cost target. The amount of lignin retained on/in LCNM can be tuned by adjusting the fractionation severity to achieve the desired physical and chemical properties as well as to meet the respective market demands for LCNM and LNP. Compared with many existing lignocellulose fractionation technologies,[35–38] we believe that the present low temperature and atmospheric pressure acid hydrotrope chemistry for producing high value LCNM and LNP holds greater potential in achieving commercial success. We are not aware of any similar work being reported in the literature; the only relevant work on producing LCNM directly from lignocelluloses uses SO_2-ethanol organosolv pulping[39] that was proven to be expensive by the pulp and paper industry in the 1980s in addition to the environmental concerns over SO_2 air emission.

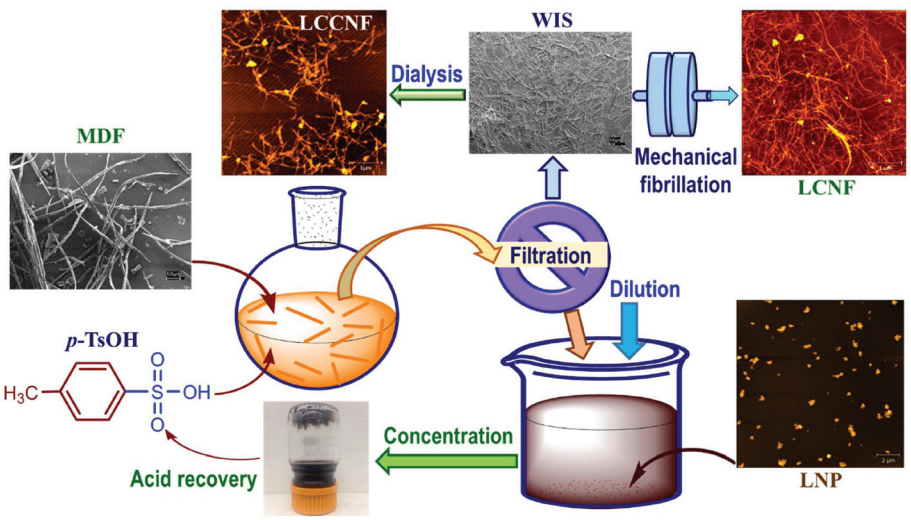

Fig. 1 A schematic process flow diagram illustrating the fractionation of medium density wood fiberboard fibers (MDF) for producing lignocellulosic crystalline nanofibrils (LCCNF), lignocellulosic nanofibrils (LCNF), and lignin nanoparticles (LNP) using *p*-toluenesulfonic acid (*p*-TsOH).

Results and discussion

Chemical compositions and yields of fractionated water insoluble solids

Medium density fiberboard fibers (MDF), produced from birch wood chips through pressurized mechanical refining, were used for this fractionation study using *p*-TsOH at 3 different concentrations. To facilitate discussion, fractionated MDF samples were labelled using their respective abbreviated fractionation conditions as PxxT80t20 to represent the *p*-TsOH concentration in xx (50, 65, 80) wt% at temperature 80 °C for 20 min. The washed WIS from each *p*-TsOH fractionation was separated from the spent acid liquor through filtration (Fig. 1) and then dialyzed using de-ionized (DI) water until the conductivity of the liquid approached to that of DI water at approximately 2 μS cm^{-1}. The WIS chemical composition and mass balance from each fractionation are listed in Table 1. Increasing fractionation severity (or *p*-TsOH concentration here) increased lignin solubilization and xylan dissolution, but reduced the WIS yield. Approximately 85% of the birch wood lignin and 70% of xylan were solubilized at P80T80t20 with a WIS yield of approximately 51%. Cellulose losses were minimal at 5% or less. The great selectivity of solubilizing lignin over the dissolution of cellulose resulted in a cellulose-rich WIS and a spent acid liquor primarily containing dissolved lignin and acid. Both WIS and dissolved lignin can be separately valorized as will be discussed in the following text.

Morphologies of lignocellulosic nanomaterials

The fractionation results presented above indicate that *p*-TsOH is not effective in hydrolyzing cellulose at low temperatures even with high concentrations. As a result, concentrated *p*-TsOH acid hydrolysis does not produce crystal-like cellulose nanomaterials, or CNC, which are often obtained after dialyzing WIS when using concentrated mineral acids[12,15] or other organic acids[16,18,19] to hydrolyze cellulosic materials. The LCNM, recovered from the supernatant of the dialyzed WIS through centrifugation, was fibril-like as shown in the left panel of Fig. 2 with lengths of over 1 μm. This perhaps can also be attributed to the absence of cellulose consolidation into the crystalline material through the MDF production process.[40] Globular-shaped lignin particles were also visible. Despite a substantial amount of disordered cellulose remaining after hydrolysis, we believe these fibril-like materials should have a higher crystallinity than the feed fibers since *p*-TsOH dissolved a substantial amount of hemicelluloses and hydrolyzed some fast reaction cellulose. To differentiate this material from LCNF derived from the mechanical fibrillation of partially hydrolyzed fibers in WIS after *p*-TsOH treatment, we can call this fibril-like material lignin containing cellulose crystalline nanofibrils (LCCNF). Because of the low yield, the amount of LCCNF obtained was not sufficient for crystallinity measurements. At the lowest *p*-TsOH concentration of 50 wt%, the yield of LCCNF was near zero (no atomic force microscopy (AFM) image in Fig. 2). Increasing the *p*-TsOH concentration resulted in better fibril separation, and therefore thinner and more uniform LCCNF diameters with a longer length. This can be observed by comparing the two AFM images in the left panel of Fig. 2b and c, and AFM topographic measured height distributions in the right panel of Fig. 2b and c. The estimated aspect ratios were 20 and 75 for LCCNF from P65T80t20 and P80T80t20, respectively. The AFM images (left panel) seem to indicate that the LCCNF is stiffer with less curvature than its corresponding LCNF (middle panel).

Subsequent mechanical fibrillation of the washed WIS, after separating LCCNF through dialysis, produced LCNF. The morphology of LCNF varied with the severity of *p*-TsOH hydrolysis as shown by AFM in the middle panel of Fig. 2. Some small, globular-shaped lignin particles were visible especially at low severity fractionation. Increasing hydrolysis severity (or *p*-TsOH concentration) resulted in less entangled LCNF with thinner diameters as observed from the AFM images and AFM measured height distributions (right panel of Fig. 2). The mean LCNF fibril height decreased from 51.1 to 29.4, and 15.3 nm when the acid concentration was increased from 50 to 65 and 80 wt%, respectively. The lignin (including the separated globular lignin particles) contents of these three LCNF samples were 16.0, 11.6, and 7.2% (Table 1). This suggests that higher residual lignin content impeded mechanical fibrillation, contradictory to the results found in the literature using unbleached softwood[20] and hardwood[19] chemical pulps. Perhaps the lignin after acid hydrolysis in the present samples may have some degree of condensation compared to lignin from organosolv[20] and kraft pulping.[19] Spence *et al.*[41] reported a LCNF mean diameter of 85 nm produced from a unbleached hardwood chemical pulp of lignin content 2.4% using extensive mechanical preprocessing, *i.e.*, 20 passes through microfluidization. Our previous study[19] reported two LCNF of approximately 10 and 7 nm in height (diameter). These two LCNF samples were produced using concentrated maleic acid

Table 1 List of chemical compositions and yields of *p*-TsOH fractionated washed water insoluble solids (WIS) from different hydrolysis conditions along with those of the untreated medium density fiberboard fibers (MDF). The numbers in the parentheses are yields based on original components in MDF. ND = not detected

Sample abbreviation	Glucan (%)	Xylan (%)	Mannan (%)	Galactan (%)	Arabanan (%)	Klason lignin (%)	WIS yield (%)
MDF	35.32	20.52	1.89	1.03	0.40	23.47	100
WIS-P50T80t20	59.24 ± 0.96 (95.0)	14.99 ± 0.28 (41.1)	2.35 ± 0.02 (70.5)	ND	ND	15.96 ± 0.47 (38.5)	56.66
WIS-P65T80t20	62.03 ± 0.74 (95.1)	13.99 ± 0.12 (36.9)	2.60 ± 0.01 (74.5)	ND	ND	11.64 ± 0.32 (26.9)	54.15
WIS-P80T80t20	67.71 ± 0.20 (98.4)	12.17 ± 0.08 (30.4)	2.50 ± 0.07 (67.9)	ND	ND	7.18 ± 0.18 (15.7)	51.31

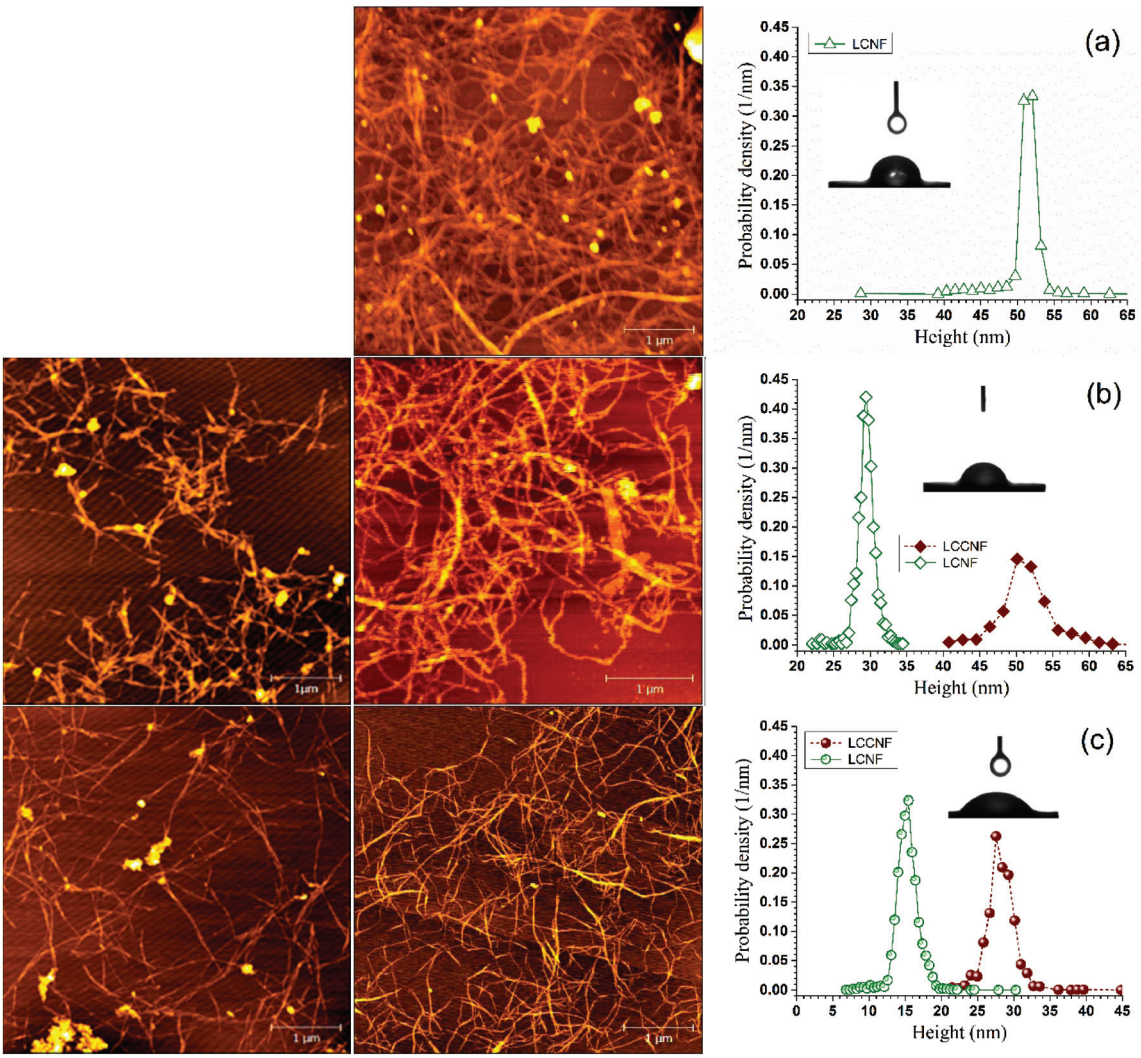

Fig. 2 Effects of the severity of *p*-toluenesulfonic acid fractionation on the morphologies of the resulting lignocellulosic crystalline nanofibrils (LCCNF) and lignocellulosic nanofibrils (LCNF) measured by atomic force microscopy (AFM), along with interaction images of the water droplet with LCNF pellets. All LCNF were from 5 passes through the 87 μm chamber of the Microfluidizer. All scale bars = 1 μm. Left column: LCCNF; Middle column: LCNF; Right column: AFM measured LCCNF and LCNF height distributions and interaction images of water droplet impinging onto LCNF pellets. (a) P50T80t20; (b) P65T80t20; (c) P80T80t20.

hydrolysis of two commercial unbleached virgin hardwood kraft pulps of lignin content 3.9 and 17.2%, respectively, with 5 passes through microfluidization. Although comparing LCNF reported in this study with those in the literature can be misleading due to the differences in the initial fibers and processing conditions, such comparisons suggest that the present method is effective.

The dialyzed WIS from P50T80t20 was fibrillated under varied numbers of passes through microfluidization to study the extent of mechanical fibrillation on the LCNF morphology. Additional passes resulted in reduced LCNF diameters and less entanglement as shown by the AFM images in Fig. 3a–e. The AFM measured fibril height distributions clearly show the thinning of the fibril with more passes (Fig. 3f). The mean LCNF height was reduced from 70 to, 65.2, 51.1, 22.5, 14.3 nm after increasing the numbers of passes through the 87 μm chamber of the microfluidizer from 1 to, 3, 5, 7, and 9, respectively. Furthermore, the LCNF became more uniform in diameter with more fibrillation (Fig. 3f).

Properties of lignocellulosic nanofibrils

The water retention value (WRV) of cellulosic materials can represent their porosities and interactions with water.[42] LCNF are bundles of elementary fibrils and contain pores especially after the dissolution of lignin and hemicelluloses. Comparing MDF with the LCNF samples, WRV was substantially increased with fibrillation (Table 2), *i.e.*, from 67 for MDF to over 300 for all LCNF samples, this is probably also due to the increased surface area through fibrillation. Increasing *p*-TsOH hydrolysis severity increased WRV due to the reduced lignin content that reduced the fibril hydrophobicity (Table 2) and increased the porosity, as well as improved fibril separation that resulted in

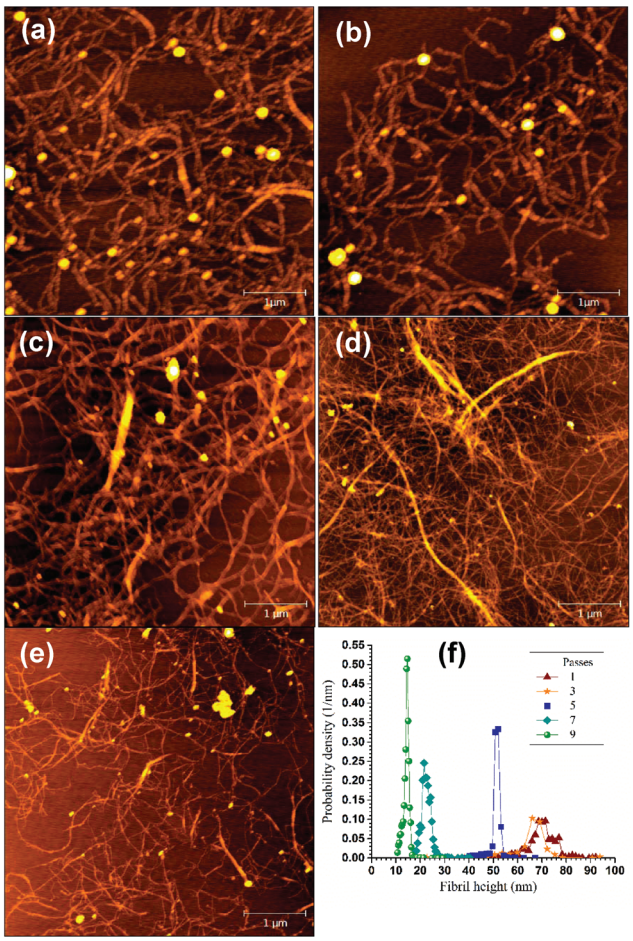

Fig. 3 Effects of the degree of mechanical fibrillation, measured by the number of passes through the 87 μm chamber of the microfluidizer, on the morphology of the resulting lignocellulosic nanofibrils (LCNF). LCNF were produced using *p*-toluenesulfonic acid fractionated lignocellulosic solids residue (LCSR) at P50T80t20 after passing through a 200 μm chamber for 3 passes at 40 MPa and a 87 μm chamber from 1 to 9 passes at 120 MPa. All scale bars = 1 μm. (a) 1 pass, mean height = 70.0 nm; (b) 3 passes, mean height = 65.2 nm; (c) 5 passes, mean height = 51.1 nm; (d) 7 passes, mean height = 22.5 nm; and (e) 9 passes, mean height = 14.3 nm. (f) Comparisons of the AFM measured LCNF fibril height distributions.

thinner fibrils (middle panel in Fig. 2) and therefore a greater surface area. WRV was approximately 400 for LCNF from P80 T80t20, or approximately 6 times that of MDF. Lignin in the cell wall can control the water content by shielding the free accessible hydroxyl group from the formation of hydrogen bonding with water molecules to result in reduced WRV.[41] Again WRV was not measured for LCCNF due to the limited quantities of materials produced.

The crystallinity indices (CrI) of the LCNF samples are substantially higher than the CrI of the MDF (Table 2) despite the fact that mechanical fibrillation can break-up cellulose crystals to reduce crystallinity, because *p*-TsOH hydrolysis dissolved substantial amounts of amorphous lignin and hemicelluloses. Even with lignin and xylan contents of 7.2 and 12.2%, respectively, the CrI of the LCNF-P80T80t20 was 68.8%. These results provide support for our suggestion that the fibril-like nanomaterials, LCCNF, directly separated from the *p*-TsOH hydrolyzed WIS prior to mechanical fibrillation are highly crystalline.

LCNF should be hydrophobic in comparison with lignin free samples. The initial water contact angles (WCA) of the three LCNF samples were measured by dropping water droplets on LCNF pellets (right panel in Fig. 2). The effect of the pellet surface roughness on the WCA was corrected for by the Wenzel equation using the measured average surface roughness. The average WCA of the initial MDF was only 30° (Table 2). Nanofibrillation increased hydrogen bonding among fibrils which reduces the porosity of LCNF pellets to result in a substantially higher WCA than that of MDF even though the lignin content of LCNF was lower than that of MDF. Among the LCNF samples, the WCA was higher for samples with a greater lignin content (Table 2). The WCA was increased from 47° for LCNF-P80T80t20 with a lignin content of 7.2% to 82° for LCNF-P50T80t20 with a lignin content of 16.0%, suggesting that LCNF can have excellent hydrophobicity.

The zeta-potentials of the LCNF samples were not much different from that of the MDF (Table 2), suggesting that *p*-TsOH only acted as a catalyst and did not induce the formation of new charged functional groups in undissolved carbohydrates. This can be verified from the comparison of the FTIR spectra between the MDF and LCNF-P80T80t20 specimen (Fig. S2†). Small variations in the lignin region were due to the dissolution of lignin.

LCNF also have good thermal stability based on thermogravimetric analysis (TGA) because lignin is more thermally stable than cellulose (Fig. S3†). The maximum degradation temperatures T_{max} of LCNF and MDF samples, derived from the derivative TGA data, are listed in Table 2. The T_{max} for the MDF with a lignin content of 23.5% was 394 °C, higher than those for LCNF with lignin contents below 16%. The increased surface area from nanofibrillation may have facilitated

Table 2 Physical, chemical, and thermal properties of the LCNF samples produced under various *p*-TsOH fractionation conditions in comparison with those of untreated MDF. Standard deviations in the water contact angle measurements were less than 2°

Sample abbreviation	Klason lignin (%)	Average height (nm)	WRV (%)	CrI (%)	Zeta potential (mV)	Water contact angle (°)	T_{max} (°C)
MDF	23.5		67	54.6	−18.2 ± 2.7	30	394
LCNF-P50T80t20	16.0	51.1	318	64.3	−23.4 ± 1.2	82	358
LCNF-P65T80t20	11.6	29.4	347	67.5	−17.9 ± 2.0	70	356
LCNF-P80T80t20	7.2	15.3	398	68.8	−20.7 ± 1.0	47	338

increased thermal degradation. Among the three LCNF samples, LCNF-P50T80t20 with a lignin content of 16.0% had the highest T_{max} of approximately 358 °C compared to the other two LCNFs prepared through more severe acid hydrolysis (Table 2). It appears that the LCNF samples have a higher onset degradation temperature (defined at which $dW/dT = 1\%$) than MDF (Fig. S3†).

The above analyses clearly indicate that the chemical compositions, yields, morphologies, and physical and thermal properties of LCNF can be tailored by controlling the reaction severity (*e.g.*, acid concentration, temperature, and time). The morphologies of LCNF can also be controlled by the intensity of mechanical fibrillation.

Properties of LPN

The dissolved lignin (Fig. S4†) in the hydrolysate, or spent *p*-TsOH liquor, can be separated simply through precipitation after diluting the spent acid liquor to below the MHC. Repeated centrifugation of the precipitated lignin and removal of the clear supernatant ultimately resulted in a turbid suspension, suggesting the presence of LNP. The LNP suspension was then dialyzed to further remove the residual *p*-TsOH. The dialyzed LNP suspensions (shown in the left bottle of Fig. 4a) were analyzed for size, zeta potential and molecular weight. The *p*-TsOH fractionation severity (acid concentration only in the present study) was found to affect the resultant LNP physical and chemical properties. The dynamic light scattering (DLS) measured average LNP particle size decreased with increasing *p*-TsOH concentration (Table 3, Fig. S5†). The DLS size was reduced from 344 to 258 nm when the acid concentration was increased from 50 to 80 wt% at the same fractionation temperature and duration. The DLS measured size distribution polydispersity index was also slightly reduced. The zeta-potentials of the LNP were not much affected by the fractionation severity, having values of approximately −30 mV (Table 3). Molecular weight distributions determined by gel-permeation chromatography (GPC) indicate that all LNP samples have bimodal distributions (Fig. 4b). The weight averaged LNP molecular weight M_w was decreased from approximately 7200 to 3100 when the acid concentration was increased from 50 to 80 wt% (Table 3). The LNP can aggregate upon drying (Fig. 4c). Particle sizes as large as 100 μm were observed from the freeze-dried SEM images (Fig. 4d Fig. S6†).

The dialyzed LNP in suspension was centrifuged to study their morphology using AFM. Centrifugation was able to remove large LNP or LNP aggregates to result in a supernatant containing small and uniform LNP. The AFM measured LNP height distributions indicated that a greater centrifugation force resulted in a narrower distribution with a smaller average height as shown in Fig. 4e, as well as less LNP aggregates with a smaller lateral size as shown in Fig. 4f–j. A monodisperse LNP height distribution was obtained using 15 000 rpm centrifugation with a mean height of 7 nm (Fig. 4e), suggesting that these LNPs in the suspension are not aggregates, but rather primary lignin particles; the corresponding lateral size was approximately 150 nm. This indicates that the non-aggre-

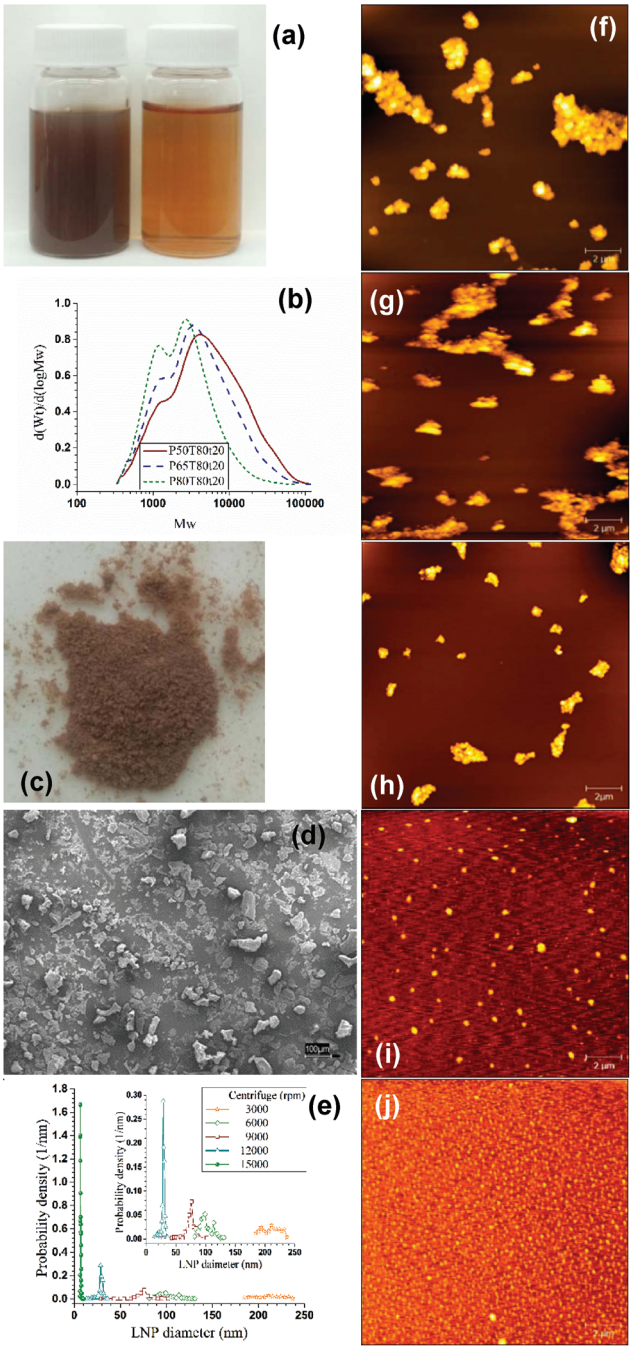

Fig. 4 Characteristics of lignin nanoparticles (LNP) produced through precipitation after diluting the spent acid liquor from P80T80t20 to below the minimal hydrotrope concentration (MHC) followed by dialysis. (a) Left bottle: images of dialyzed LNP suspension, right bottle: the supernatant from centrifuging the suspension in the left bottle at 10 000 rpm for 10 min. (b) Comparisons of the molecular weight distributions of the dialyzed LNP from *p*-toluenesulfonic acid fractionations at different severities. (c) A photograph of freeze-dried LNP from the left bottle in (a). (d) SEM image of the LNP in (c), scale = 100 μm. (e)–(j): LNP in the supernatants from centrifuging the suspension in the left bottle of (a) at different speeds for 10 min; (e) comparisons of atomic force microscopy (AFM) measured height distributions; (f)–(j) AFM topographic images, scale = 2 μm: 3000 rpm, mean height = 210.3 nm (f); 6000 rpm, mean height = 100.8 nm (g); 9000 rpm, mean height = 73.9 nm (h); 12 000 rpm, mean height = 28.7 nm (i); 15 000 rpm mean height = 7.0 nm (j).

Table 3 Physical and chemical properties of the lignin nanoparticles (LNP) from dissolved lignin under three *p*-TsOH fractionation conditions

Sample abbreviation	DLS diameter (nm)	Polydispersity index	Zeta potential (mV)	Molecular weight		
				M_w	M_n	M_w/M_n
LNP-P50T80t20	344.1 ± 8.9	0.184	−31.7 ± 2.2	7228	2373	3.05
LNP-P65T80t20	287.2 ± 4.0	0.175	−30.2 ± 0.8	5265	2002	2.63
LNP-P80T80t20	258.1 ± 3.3	0.163	−27.2 ± 1.5	3052	1571	1.94

gated primary LNP are oblate spheroid nanoparticles and centrifugation is able to fractionate LNP according to their size.

Conclusions

This study demonstrated a promising pathway for low-cost and sustainable production of wood-based nanomaterials such as LCNF and LNP directly from wood using a recyclable acid hydrotrope, *p*-TsOH. *p*-TsOH can rapidly and efficiently solubilize up to 85% of birch wood lignin at 80 °C for only 20 min resulting in a carbohydrate-rich water insoluble solid fraction and a spent liquor stream mainly containing dissolved lignin. LNP was produced simply by diluting the spent liquor to below the *p*-TsOH MHC of approximately 10%. AFM imaging analyses indicate that the primary LNP are oblate spheroid nanoparticles of approximately 150 nm in lateral size and 7 nm in thickness. These elemental particles can aggregate into large particles of several micrometers in length and 200 nm in thickness. LCNF produced from subsequent mechanical fibrillation of WIS, after separating a small amount of lignin-containing cellulose crystalline fibrils, were entangled with uniform diameters between 15 and 51 nm and varied hydrophobicity. The morphological, physical, and chemical properties of LCNF and LNP can be tailored by adjusting the fractionation severity. *p*-TsOH has low solubility at ambient temperature, which facilitates efficient recovery using commercially proven crystallization technology by simply cooling the re-concentrated spent acid solution after lignin precipitation. The pathway we presented here has a substantial impact on the economic, sustainable, and high value utilization of the abundant, renewable, and biodegradable lignocelluloses.

Methods and materials

Materials

A birch (*B. papyrifera*) tree of approximately 35 years of age was harvested from the Rhinelander Experimental Forest in Rhinelander, WI, USA, and provided by Dr Ronald Zalesny, Jr. from the Institute for Applied Ecosystem Studies of the USDA Forest Service Northern Research Station. Logs of the tree were 1.2–1.8 m in length with diameters between 15 and 23 cm and were transported to the USDA Forest Products Laboratory, Madison, WI. After manual debarking, the logs were chipped using a 127 cm diameter, 45 kW knife-chipper (Carthage Machine Co, Carthage, NY). The chips were processed through a vibratory screen to remove particles larger than 38 mm and less than 6 mm. The thickness of the accepted chips ranged from 1 to 5 mm. The moisture content of the accepted wood chips was 61%. The chips were refrigerated at 4 °C until use.

p-TsOH was ACS reagent grade and purchased from Sigma-Aldrich (St. Louis, MO). Dialysis bags with a typical cut-off molecular weight of 14 000 Da were also from Sigma-Aldrich (Product No. D9402-100FT). Filter paper (15 cm, slow) was from Fisher Scientific Inc. (Pittsburgh, PA).

MDF

MDFs were produced by refining birch wood chips in a 30.5 cm pressurized disk refiner (Sprout-Bauer, model 1210P, Muncy, PA, USA) with disk plate patterns of D2B505 and a disk gap of 0.178 mm. The wood chips were pre-steamed at 165 °C for 10 min with a steam pressure of 0.72 MPa. The refining feed rate was approximately 1 kg min^{-1} on oven dry (OD) weight basis. The refining energy input was 127 Wh kg^{-1} OD chips. The resulting pulp fibers were stored in a plastic bag for further processing.

Fractionation of MDF using *p*-TsOH hydrolysis

A *p*-TsOH solution of desired concentration was prepared by mixing the required amounts of *p*-TsOH and DI water in a three-necked flask. The *p*-TsOH solution in the flask was then heated in a glycerol bath to 80 °C on a heating plate, as described previously.[17] MDF of 5 g (in OD weight) was manually fed into the completely dissolved acid solution resulting in a liquor to MDF mass ratio of 20 : 1. The fiber suspension was constantly mixed using a mechanical mixer at 300 rpm. Reactions were conducted at *p*-TsOH concentrations of 50, 65, and 80 wt% at 80 °C for 20 min. At the end of each reaction, 100 mL of DI water was added to quench the reaction. The hydrolysate was then separated by vacuum filtration through a filter paper. The filter cake was further washed using DI water and collected as WIS (Fig. S7†) for chemical composition analysis and LCNF production. The filtrate was collected for recovery of acid and dissolved lignin.

Productions of LCCNF and LCNF

The collected WIS was dialyzed to separate the LCCNF. The resulting partially hydrolyzed lignocellulosic residue (LCSR) was mechanically fibrillated by feeding its suspension at 1% into a microfluidizer (M-110EH, Microfluidics Corp., Westwood, MA). The fiber suspension was first passed through a 200 μm chamber for 3 passes at 40 MPa (Fig. S8†), and then

additional 1–9 passes through an 87 μm chamber at 120 MPa (Fig. 3).

Separation of LNP

The collected hydrolysate (filtrate) was diluted using DI water to approximately 10 wt% acid concentration that is below the minimal *p*-TsOH hydrotrope concentration (MCH). Precipitation of dissolved lignin was observed at the bottom of the solution. The diluted spent acid liquor was centrifuged at 10 000 rpm (16 264 *g*) for 10 min (Sorvall Superspeed RC2-B, GSA rotator, Ivan Sorvall, Inc., Norwalk, CT) to remove excess acid by removing the clear supernatant. This dilution and centrifuging process was repeated until the supernatant became turbid, suggesting that most dissolved lignin had been aggregated as nanoparticles. An aliquot sample was then taken after mixing the turbid LPN suspension for analyses by SEM, AFM, GPC, zeta-potential, and DLS particle sizing.

To study the LNP morphology and the effect of the centrifugation speed on size fractionation of LNP, the turbid LNP suspensions were dialyzed. The dialyzed LNP suspensions were then centrifuged at different speeds using a different rotor, SS-34, in the same centrifuge described above (Sorvall Superspeed RC2-B).

Analyses and characterization

The chemical compositions of MDF and washed WIS samples from different fractionation severities were hydrolyzed using sulfuric acid in two steps for carbohydrate and Klason lignin analyses by the Analytical Chemistry and Microscopy Lab (ACML) at the Forest Products Lab, as described previously.[43]

Drops of aqueous suspensions of washed WIS and dialyzed LNP were air-dried and freeze-dried, respectively, on well-polished aluminum mounts before scanning electron microscopy (SEM) analyses. All SEM samples were sputter-coated with gold to provide adequate conductivity. Images were observed and recorded using a Leo EVO 40 SEM (Carl Zeiss NTS, Peabody, MA) under ultrahigh vacuum conditions.

Morphologies of LCNF and LNP were analyzed using AFM (AFM workshop, Signal Hill, CA, USA). Briefly, suspensions with approximately 0.01 wt% concentration were deposited on mica substrates and air-dried at ambient temperature. AFM topographical images were obtained in tapping mode at 160–225 kHz using a silicon cantilever and a tip with a radius of curvature of 10–15 nm. The height distributions of LCNF and LNP were analyzed using Gwyddion software (Department of Nanometrology, Czech Metrology Institute, Crezh Republic, 64-bit).

The water retention value (WRV) of the MDF and LCNF were measured according to the Scandinavian test method SCAN-C 62 : 00[44] as described in our previous study.[45]

The crystal structure of the LCNF was analyzed by using an X-ray diffractometer (Bruker D8 130 Discover, Bruker Corp., Billerica, MA, USA) with Cu-Kα radiation. Samples were pressed at 180 MPa to make pellets. Scattering radiation from a pellet made of freeze-dried LCNF was detected in a 2θ range from 10° to 38° in steps of 0.02°. As described previously, the crystallinity index (CrI) was calculated in accordance with the Segal method (without baseline subtraction).[46]

The surface charge of the LCNF and the effective diameter of LNP were measured using a dynamic light scattering analyzer (DLS, Nanobrook Omni, Brookhaven Instruments, Holtsville, NY) at ambient temperature. The concentration of the suspensions was approximately 0.5 and 0.05 g L^{-1} for LCNF and LNP, respectively. Five measurements were carried out for each sample and the averages were reported.

The static water contact angles (WCA) of MDF and LCNF samples were measured by the sessile drop method using a contact angle analyzer (Attention Theta, Biolin Scientific, Inc. Stockholm, Sweden). Samples were first pressed at 180 MPa to make pellets and placed on the sample stage. A drop of distilled water of approximately 8 μL was automatically dispensed onto the surface of a pellet from a micro syringe. The image of the water droplet was recorded right at the instant when the drop touched the pellet surface. Curve fitting and data analysis were performed using the OneAttension software provided with the instrument. Three measurements were made for each sample and an average was presented.

For lignin molecular weight measurements, a freeze-dried lignin sample of 0.1 g from the mixed turbid LNP suspension was dissolved in 2 mL of pyridine-acetic anhydride (1 : 1 by volume) solution and kept in a dark cabinet at room temperature for three days. The solution was added dropwise into 120 mL of ice-cold water containing 1 mL of concentrated HCl with constant stirring. The precipitated lignin acetate was collected on a 10 μm nylon membrane by filtration, washed with water, and dried in air and then under vacuum. The number-average and weight-average molecular weights (M_n and M_w, respectively) of the acetylated lignin samples were estimated using GPC on an ICS-3000 system (Dionex, Sunnyvale, CA) with three 300 mm × 7.8 mm (i.d.) Phenogel 5U columns (10 000, 500, and 50 Å) and a 50 mm × 7.8 mm (i.d.) Phenogel 5U guard column (Phenomenex, Torrance, CA). Lignin acetate of 5 mg was dissolved in 1 mL of HPLC-grade tetrahydrofuran (THF) without a stabilizer, and 50 μL of the resulting solution was injected into the GPC columns. THF was used as the eluent at a flow rate of 1 mL min^{-1}. The column temperature was 30 °C. Polystyrene standards were used for calibration. Lignin samples and polystyrene standards were detected using a variable wavelength detector (VWD) at 280 and 254 nm, respectively.

The thermal properties of the LCNF samples were analyzed using a thermogravimetric analyzer (Pyris 1, PerkinElmer, Inc., Waltham, MA). Freeze-dried LCNF samples of roughly 5 mg were weighed and heated from ambient temperature to 700 °C at a heating rate of 10 °C min^{-1} under a high purity N_2 stream of 20 mL min^{-1}.

Acknowledgements

This work was conducted on the official US government time of Zhu and Gleisner. The financial support from the US Forest

Service made the visiting appointments of Bian and Chen at the US Forest Service, Forest Product Lab possible. Bian also would like to acknowledge the financial support from the Chinese State Forestry Administration (Project No. 2015-4-54), the National Natural Science Foundation of China (Project No. 31470599), and the Doctorate Fellowship Foundation of Nanjing Forestry University. We also would like to acknowledge Prof. Xuejun Pan and his Ph.D student Ning Li of the University of Wisconsin, Madison for conducting GPC measurements in his laboratory and Dr Ronald Zalesny, Jr. and his staff from the Institute for Applied Ecosystem Studies, USDA Forest Service Northern Research Station, for harvesting the birch tree.

References

1 S. J. Eichhorn, A. Dufresne, M. Aranguren, N. E. Marcovich, J. R. Capadona, S. J. Rowan, C. Weder, W. Thielemans, M. Roman, S. Renneckar, W. Gindl, S. Veigel, J. Keckes, H. Yano, K. Abe, M. Nogi, A. N. Nakagaito, A. Mangalam, J. Simonsen, A. S. Benight, A. Bismarck, L. A. Berglund and T. Peijs, *J. Mater. Sci.*, 2010, **45**, 1–33.
2 S. S. Nair, S. Sharma, Y. Pu, Q. Sun, S. Pan, J. Y. Zhu, Y. Deng and A. J. Ragauskas, *ChemSusChem*, 2014, **7**, 3513–3520.
3 R. J. Moon, A. Martini, J. Nairn, J. Simonsen and J. Youngblood, *Chem. Soc. Rev.*, 2011, **40**, 3941–3994.
4 C. Jiang, H. He, H. Jiang, L. Ma and D. M. Jia, *eXPRESS Polym. Lett.*, 2013, **7**, 480–493.
5 A. Mulyadi, Z. Zhang, M. Dutzer, W. Liu and Y. Deng, *Nano Energy*, 2017, **32**, 336–346.
6 H. Zhu, W. Luo, P. N. Ciesielski, Z. Fang, J. Y. Zhu, G. Henriksson, M. E. Himmel and L. Hu, *Chem. Rev.*, 2016, **116**, 9305–9374.
7 X. Xu, J. Zhou, L. Jiang, G. Lubineau, T. Ng, B. S. Ooi, H.-Y. Liao, C. Shen, L. Chen and J. Y. Zhu, *Nanoscale*, 2016, **8**, 12294–12306.
8 W. Zhang, X. Zhang, C. Lu, Y. Wang and Y. Deng, *J. Phys. Chem. C*, 2012, **116**, 9227–9234.
9 J. A. Kelly, A. M. Shukaliak, C. C. Y. Cheung, K. E. Shopsowitz, W. Y. Hamad and M. J. MacLachlan, *Angew. Chem., Int. Ed.*, 2013, **52**, 8912–8916.
10 A. Querejeta-Fernández, B. Kopera, K. S. Prado, A. Klinkova, M. Methot, G. Chauve, J. Bouchard, A. S. Helmy and E. Kumacheva, *ACS Nano*, 2015, **9**, 10377–10385.
11 P. Figueiredo, K. Lintinen, A. Kiriazis, V. Hynninen, Z. Liu, T. Bauleth-Ramos, A. Rahikkala, A. Correia, T. Kohout, B. Sarmento, J. Yli-Kauhaluoma, J. Hirvonen, O. Ikkala, M. A. Kostiainen and H. A. Santos, *Biomaterials*, 2017, **121**, 97–108.
12 M. S. Reid, M. Villalobos and E. D. Cranston, *Langmuir*, 2017, **33**, 1583–1598.
13 Q. Q. Wang, J. Y. Zhu, R. S. Reiner, S. P. Verrill, U. Baxa and S. E. McNeil, *Cellulose*, 2012, **19**, 2033–2047.
14 Q. Wang, X. Zhao and J. Y. Zhu, *Ind. Eng. Chem. Res.*, 2014, **53**, 11007–11014.
15 L. Chen, Q. Wang, K. Hirth, C. Baez, U. P. Agarwal and J. Y. Zhu, *Cellulose*, 2015, **22**, 1753–1762.
16 L. Chen, J. Y. Zhu, C. Baez, P. Kitin and T. Elder, *Green Chem.*, 2016, **18**, 3835–3843.
17 H. Bian, L. Chen, R. Wang and J. Y. Zhu, *J. Visualized Exp.*, 2017, 55079, DOI: 10.3791/55079.
18 R. Wang, L. Chen, J. Y. Zhu and R. Yang, *ChemNanoMat*, 2017, **3**, 328–335.
19 H. Bian, L. Chen, H. Dai and J. Y. Zhu, *Carbohydr. Polym.*, 2017, **167**, 167–176.
20 E. Rojo, M. S. Peresin, W. W. Sampson, I. C. Hoeger, J. Vartiainen, J. Laine and O. J. Rojas, *Green Chem.*, 2015, **17**, 1853–1866.
21 I. C. Hoeger, S. S. Nair, A. J. Ragauskas, Y. Deng, O. J. Rojas and J. Y. Zhu, *Cellulose*, 2013, **20**, 807–818.
22 Q. Q. Wang, J. Y. Zhu, R. Gleisner, T. A. Kuster, U. Baxa and S. E. McNeil, *Cellulose*, 2012, **19**, 1631–1643.
23 T. Saito, Y. Nishiyama, J. L. Putaux, M. Vignon and A. Isogai, *Biomacromolecules*, 2006, **7**, 1687–1691.
24 Y. Qin, X. Qiu and J. Y. Zhu, *Sci. Rep.*, 2016, **6**, 35602.
25 H. Sehaqui, K. Kulasinski, N. Pfenninger, T. Zimmermann and P. Tingaut, *Biomacmolecules*, 2017, **18**, 242–248.
26 W. Wang, R. C. Sabo, M. D. Mozuch, P. Kersten, J. Y. Zhu and Y. Jin, *J. Polym. Environ.*, 2015, **23**, 551–558.
27 M. Pääkko, M. Ankerfors, H. Kosonen, A. Nykänen, S. Ahola, M. Österberg, J. Ruokolainen, J. Laine, P. T. Larsson, O. Ikkala and T. Lindström, *Biomacromolecules*, 2007, **8**, 1934–1941.
28 C. Frangville, M. Rutkevicius, A. P. Richter, O. D. Velev, S. D. Stoyanov and V. N. Paunov, *Chemphyschem*, 2012, **13**, 4235–4243.
29 A. P. Richter, B. Bharti, H. B. Armstrong, J. S. Brown, D. Plemmons, V. N. Paunov, S. D. Stoyanov and O. D. Velev, *Langmuir*, 2016, **32**, 6468–6477.
30 M. Lievonen, J. J. Valle-Delgado, M. L. Mattinen, E. L. Hult, K. Lintinen, M. A. Kostiainen, A. Paananen, G. R. Szilvay, H. Setälä and M. Österberg, *Green Chem.*, 2016, **18**, 1416–1422.
31 Y. Qian, Q. Zhang, X. Q. Qiu and S. P. Zhu, *Green Chem.*, 2014, **16**, 4963–4968.
32 M. Ago, S. Huan, M. Borghei, J. Raula, E. I. Kauppinen and O. J. Rojas, *ACS Appl. Mater. Interfaces*, 2016, **8**, 23302–23310.
33 R. H. McKee, *US Patent*, 2308564, 1943.
34 K. Gabov, R. J. A. Gosselink, A. I. Smeds and P. Fardim, *J. Agric. Food Chem.*, 2014, **62**, 10759–10767.
35 A. Brandt, M. J. Ray, T. Q. To, D. J. Leak, R. J. Murphy and T. Welton, *Green Chem.*, 2011, **13**, 2489–2499.
36 J. Y. Zhu, X. J. Pan, G. S. Wang and R. Gleisner, *Bioresour. Technol.*, 2009, **100**, 2411–2418.
37 M. Iakovlev and A. van Heiningen, *ChemSusChem*, 2012, **5**, 1625–1637.

38 J. S. Luterbacher, J. M. Rand, D. M. Alonso, J. Han, J. T. Youngquist, C. T. Maravelias, B. F. Pfleger and J. A. Dumesic, *Science*, 2014, **343**, 277–280.
39 K. Nelson, T. Retsina, V. Pylkkanen and R. O'Connor, *U.S. Patent No* 9187865B2, 2015.
40 U. P. Agarwal, S. A. Ralph, R. S. Reiner and C. Baze, *Cellulose*, 2016, **23**, 125–144.
41 K. L. Spence, R. A. Venditti, O. J. Rojas, Y. Habibi and J. J. Pawlak, *Cellulose*, 2010, **17**, 835–848.
42 X. Luo, J. Y. Zhu, R. Gleisner and H. Y. Zhan, *Cellulose*, 2011, **18**, 1339–1344.
43 X. Luo, R. Gleisner, S. Tian, J. Negron, E. Horn, X. J. Pan and J. Y. Zhu, *Ind. Eng. Chem. Res.*, 2010, **49**, 8258–8266.
44 SCAN, *Nordic Standardization Program*, 2000.
45 X. L. Luo and J. Y. Zhu, *Enzyme Microb. Technol.*, 2011, **48**, 92–99.
46 L. Segal, J. J. Creely, A. E. Martin and C. M. Conrad, *Text. Res. J.*, 1959, **29**, 786–794.